Physical Communication 43 (2020) 101215

Contents lists available at ScienceDirect

Physical Communication

journal homepage: www.elsevier.com/locate/phycom

Full length article

A discriminant analysis-based automatic ordered statistics scheme for radar systems

A.J. Onumanyi [a,*], H. Bello-Salau [b], A.O. Adejo [a], H.O. Ohize [c], M.O. Oloyede [d], E.N. Paulson [a], A.M. Aibinu [e]

[a] Department of Telecommunication Engineering, Federal University of Technology, Minna, Nigeria
[b] Department of Computer Engineering, Ahmadu Bello University, Zaria, Nigeria
[c] Department of Electrical and Electronics Engineering, Federal University of Technology, Minna, Nigeria
[d] Department of Information and Communication Science, University of Ilorin, Ilorin, Nigeria
[e] Department of Mechatronics Engineering, Federal University of Technology, Minna, Nigeria

ARTICLE INFO

Article history:
Received 14 March 2020
Received in revised form 20 September 2020
Accepted 21 September 2020
Available online 28 September 2020

Keywords:
Automatic
CFAR
Discriminant analysis
Otsu
Radar
Signal detection

ABSTRACT

The ordered statistics (OS) scheme is an effective constant false alarm rate (CFAR) technique deployed in many radar systems. It is widely deployed because of its simplicity and effectiveness under conditions of both homogeneous and non-homogeneous radar returns. However, the problem of inaccurate censoring typically degrades its performance since it is often difficult to accurately determine the actual number of interfering targets and clutter edges in the reference window per time. In this article, we address this problem based on the principle of discriminant analysis (DA) towards automatically and effectively estimating the k^{th} rank ordered element of the OS scheme. Our scheme, termed the DA-OS scheme, works without requiring *a priori* knowledge about the statistical characteristics of the input radar returns. The results obtained via Monte Carlo simulation indicate that the DA-OS scheme achieves a small CFAR loss of about 0.392 dB relative to the cell averaging (CA) scheme under conditions of homogeneous radar returns at a probability of detection of 0.5. It outperforms other notable traditional schemes, including the CA, smallest-of CA, greatest-of CA, and the fixed OS schemes under conditions of non-homogeneous radar returns. Finally, it provides a number of desirable qualitative characteristics as against other existing censoring techniques.

1. Introduction

Radar systems are highly useful in many remote sensing applications, for example, they are invaluable in the recent fourth industrial revolution, which encompasses the control of industrial robots to sense and avoid collision [1], for speed control of mobile industrial machines, monitoring of industrial environments for fault identification, location and security purposes [2], as well as for object and proximity detection [3], and in covert communications [4,5]. Other classic areas concerned with radar usage include the weather [6], agriculture [7], military, geological [8], civil [9], and aviation industries [7], to name but a few. These automotive application areas depend on radar sensors integrated with processors and controllers designed to improve the detection, safety, forecasting, security, and productivity of these respective industries [10,11]. However, in order to guarantee the effectiveness of radar systems, it is imperative to deploy effective constant false alarm rate (CFAR) schemes within such radar systems towards ensuring that their false alarm rates are kept below a predefined value to prevent erroneous operation.

There are some classic and simple CFAR schemes that can be deployed in the above-mentioned radar application areas. For example, the cell averaging (CA), smallest-of cell averaging (SOCA), greatest-of cell averaging (GOCA) are fundamental methods deployed pervasively across many radar systems [12]. Most other schemes are often derived or based on the CA and its variants [13–15]. However, the CA has a key limitation in its performance under non-homogeneous conditions, where radar returns within the reference cells contain multiple interfering targets and/or clutter returns. Under such non-homogeneous conditions, the CA scheme incurs increased false alarm rates at clutter edges as well as target masking in the presence of interfering targets. The SOCA scheme was proposed to resolve the problem of target masking under conditions of multiple interfering targets, however, it presents very high false alarm rates at clutter edges.

* Corresponding author.
E-mail addresses: adeiza1@futminna.edu.ng (A.J. Onumanyi), bellosalau@gmail.com (H. Bello-Salau), achonu@futminna.edu.ng (A.O. Adejo), henryohize@futminna.edu.ng (H.O. Ohize), tahir.oloyede@gmail.com (M.O. Oloyede), enpaulson2@gmail.com (E.N. Paulson), maibinu@gmail.com (A.M. Aibinu).

https://doi.org/10.1016/j.phycom.2020.101215
1874-4907/

On the other hand, the GOCA scheme was introduced to address the false alarm rate problem at clutter edges, however, it fails to solve the problem of target masking. Many other methods have been proposed towards realizing an all-encompassing scheme that addresses both the problem of target masking as well as false alarm rate reduction at clutter edges. However, the classic work of Weiss noted that such a scheme may almost never be developed [16, pp. 111], which has been further affirmed in [14, 17]. Notwithstanding, some other classic theoretical works have suggested that the ordered statistics (OS) scheme may suffice as a possible candidate technique capable of addressing both problems [18,19], a fact that has gained much approval from a number of past and recent practical and comparative works [20,21].

Basically, the OS scheme works by reordering the radar returns within a reference window in an ascending order based on their relative energy levels. In this article, the term "sample" and "radar returns" are often used interchangeably to refer to the entire set of received energy values of the reflected radar signal stored in the reference window. Thus, a sample typically comprises elements, where an element denotes a single discrete energy value of the radar return stored in a single cell of the reference window. Further description of the reference window is provided in Section 3.1. By ordering the elements in the reference window, the OS scheme selects a single ordered element (i.e. the kth sample element) to serve as the estimated noise value in the reference window. Essentially, because the accuracy of the estimated noise value determines the degree of effectiveness of the OS scheme, it is thus pertinent that the choice of the kth element should be determined as accurately as possible. If the kth element is accurately determined, the OS scheme typically solves the target masking problem as well as reduces the false alarm rate at clutter edges [13]. However, the existing challenge is that it is generally difficult to develop practical methods that are able to accurately and dynamically determine the kth rank ordered element of the OS scheme based on a definite metric that measures the degree of homogeneity/non-homogeneity in the reference window. Furthermore, such a method must be able to perform effectively without requiring a lookup table to determine the appropriate threshold value needed to maintain a predefined probability of false censoring. These qualitative requirements are discussed in Section 6. In this regard, the term "censoring" refers to the identification and removal of non-homogeneous radar returns present in the reference window of a CFAR scheme in order to reduce their detrimental effects on the performance of such a scheme. However, most attempts at dynamically estimating the kth rank ordered element (as highlighted in Section 2) are fraught with certain limitations (as discussed qualitatively in Section 6), which leaves ample room for further improvement and innovative ideas as introduced in the present article.

Thus, in this article, we explore a method that accurately determines the exact number of interfering targets as well as clutter edges within the reference window of the OS scheme based on the principle of discriminant analysis (DA). Our proposed scheme termed the DA-OS scheme is able to accurately estimate the number of interfering targets within a reference window without *a priori* knowledge about its operating environment and without the need to reconfigure the value of a specific probability of false censoring. Our method provides an improved performance under conditions of multiple interfering targets and clutter edges within the reference window. We compare our method against the OS scheme based on the optimum criterion posed in [22] and with other well known schemes such as the CA, SOCA, GOCA schemes. Results obtained are presented and discussed in order to demonstrate the improved performance of our approach.

The subsequent contents of this article are organized as follows: We discuss the relevant literature in Section 2. The proposed DA-OS scheme is introduced in Section 3, including its operating algorithm and time complexity analysis. Our method of simulation and analysis is presented in Section 4. Results and discussion are highlighted in Section 5, whereas a qualitative assessment of the DA-OS scheme relative to existing censoring methods is presented in Section 6. The article is concluded in Section 7.

Notation. We used upper-case letters X_N to denote a set of unordered elements, where N is the total number of elements in the set, and lower-case letters x_n denote the actual value of each element in the set, where n represents the index of each element; the set of ordered elements arranged in an ascending order is denoted by upper-case letters with a bracketed subscript $X_{(N)}$ and its corresponding nth ordered element is denoted as $x_{(n)}$; $\overline{F}$ denotes the mean of the elements in the set F; the calligraphic symbol $\mathcal{O}(\cdot)$ denotes the time complexity, whereas the symbol "$\leftarrow$" denotes a memory assignment operation; the symbol "$\sim$" means "distributed as"; $Y \sim \mathcal{CN}(0,\ \sigma^2)$ denotes a complex Gaussian distributed random variable Y with zero-mean and variance σ^2.

2. Related work

There are some methods proposed for automatic censoring of reference cells such as the automatic censored (AC) CFAR method by Himonas & Barkat [23], which simply determines whether the cell under test (CUT) is in the clear (thermal noise only) or clutter region. Note that the term "CUT" refers to the cell for which a threshold value is to be computed, which is further depicted in Section 3.1. If the CUT is determined to be in the clear region, then cells in the clutter region are censored. However, if determined to be in the clutter region, then the cells in the clear region are censored. Subsequently, only the cells in the uncensored region are combined to estimate the noise level in the test cell. In addition to being largely heuristic, this approach is quite computationally intensive and it depends on a continuous choice and change of the scaling constant in order to achieve a desired probability of false censoring. In the present context, the term *heuristic* implies that there exists no deterministic function or metric to measure the degree of homogeneity as well as non-homogeneity within the reference window, instead, such conditions of homogeneity and non-homogeneity are determined in an iterative manner based on whether the difference between the present and previous element values within a reference window exceeds a certain predefined margin or not. A similar approach to the AC was proposed in [24] called the automatic censored cell averaging (ACCA) CFAR, which differs from the AC only by computing the mean of the uncensored cells to serve as the estimated noise level in the test cell. By being based on the AC method, the ACCA-CFAR scheme inevitably inherits its limitations as well, while incurring additional complexities. An application specific ordered cell averaging-CFAR (OCA-CFAR) was proposed in [25] for detecting events in time-series signals, particularly considering its application to seismic signals. The OCA-CFAR was demonstrated to yield improved performance compared to the CA, SOCA, GOCA, and OS schemes under different window sizes and false alarm rates.

A few other automatic methods have been proposed following the introduction of the AC and ACCA methods, such as the AC-CFAR for heterogeneous Gaussian clutter (HGC) termed (AC-HGC) [13], the ACCA based on ordered data variability (ODV) termed ACCA-ODV [26], the automatic dual censoring cell-averaging (ADCCA)-CFAR [12], the generalized ordered statistics (GOS) methods combined with CA termed GOSCA, with greatest-of termed GOSGO, and with smallest-of termed GOSSO [27]. Although these methods have been shown to perform well under

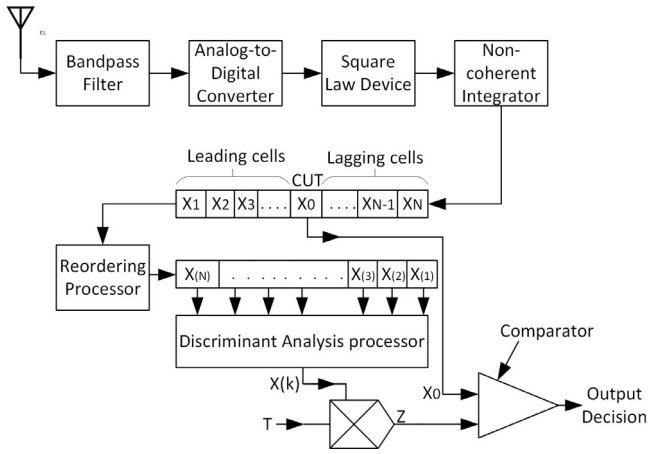

Fig. 1. Discriminant Analysis-based CFAR Scheme.

different conditions, nevertheless, they have unique limitations, for example, the ADCCA does not automatically determine the kth rank ordered element, instead, it keeps the kth element fixed, which limits its capacity for automation in the context of the present article. The AC-HGC compares the difference between adjacent elements similar to the AC and ACCA, thus being of a highly heuristic nature. The GOSCA, GOSGO, and the GOSSO do not automate the choice of the kth rank ordered element.

Above all, most censoring methods best known to us are designed to determine the first transition edge within a reference window in order to serve as the kth element for censoring purposes. Then, the residual cells above this kth point are considered to be the group of non-homogeneous elements. The inability of most censoring methods to accurately determine the exact number of interfering targets within a reference window presents a major problem, for example, if the actual number of interfering targets supersedes the estimated kth element, then the false alarm rate of the OS scheme is increased. Furthermore, it is often assumed that only a single leading clutter edge should exist within a reference window, thus, multiple clutter edges and regions may go undetected by these existing methods, which leads to an increase in the false alarm rate of the OS scheme. Different from existing methods, we introduce a new method in the present article that seeks to address the above problems based on the principle of discriminant analysis, which will be discussed in the next section.

3. Discriminant analysis-based OS CFAR scheme

In this section, we describe the DA-OS scheme and then present the motivation and working principles behind the algorithm as deployed in the scheme. This section concludes with the time complexity analysis of the DA-OS algorithm.

3.1. The DA-OS scheme

Fig. 1 presents the block diagram of the DA-OS scheme as deployed within the front-end of a typical radar system. Here, we focus on the receiver side of the system since we are concerned with detecting signals within a set of radar returns. Consequently, similar to most other schemes [18], the front-end of our DA-OS scheme consists of a single transceiver antenna (since we are concerned with the case of a monostatic radar system), a bandpass filter, the analogue-to-digital converter (ADC), the square-law device and the non-coherent integrator.

Essentially, radar returns are received via the input antenna and filtered to within the desired frequency range of the bandpass filter. The filtered elements are then digitized in the ADC block and magnitude squared in the square-law device towards obtaining the energy of each sample element. In this article, we focus on non-coherent detection as can be observed following the inclusion of the non-coherent integrator block in Fig. 1. We considered the case for non-coherent integration because most practical radar systems often work by processing a set of averaged (i.e. integrated) radar returns obtained over a sensing period towards improving the detection accuracy of radar systems. Furthermore, the integration process minimizes the required signal-to-noise ratio (SNR) needed to achieve very high detection rates for radar systems [28]. The integration block adopts a non-coherent video integration process since we are interested only in the signal's magnitude for the sake of detection and not in its phase as may be required in other application areas, for example, in the Doppler detector [28]. By adopting pulse integration, it is well known that the noise variance reduces with an increase in the number of non-coherently integrated pulses N_P, thus improving the detection rate of the scheme [28]. Possible integration techniques including the binary integration method have been well studied to improve the detection performance of radar system [29,30].

The elements of the output sample $X_N = \{x_1, x_2, x_3, \ldots, x_N\}$ from the non-coherent integrator are fed serially into a shift register wherein signal processing typically ensues. In the rest of this article, we refer to the shift register as the reference window, which determines the number of radar returns to be processed per time. By feeding the sample elements serially into the shift register, radar observers are made to visualize the reference window as though sliding in time over the range of input radar returns being fed into the register, as will be discussed in Section 5. In our design, each cell in the reference window refers to the range cell of a typical radar system. Thus, the reference window can be divided into a set of leading cells i.e $x_1, x_2, x_3, \ldots, x_{N/2}$, the cell under test (CUT) i.e. x_0, and a set of lagging cells i.e. $x_{N/2+1}, x_{N/2+2}, \ldots, x_N$. However, in most schemes, such as the CA, SOCA, GOCA and OS schemes, the radar return in the CUT is often expunged from the reference window during the computational process, and as such, only N sample elements from both the leading and lagging cells are processed per time towards computing the threshold value of the CUT. Consequently, the size of the reference window is considered to be N. Thus, Fig. 1 shows that the radar return x_0 in the CUT is expunged and passed to the comparator, while other radar returns in the reference window are passed to the reordering processor for onward processing.

In Fig. 1, the reordering processor reorders the elements of the input sample in an ascending order, where $x_{(1)} < x_{(2)} < x_{(3)} < \cdots < x_{(N)}$. These reordered elements are then passed to the DA processor, wherein the DA-OS algorithm is deployed (to be discussed in Section 3.2). The DA processor estimates the kth rank ordered sample element and outputs the radar return $x_{(k)}$ at the kth cell. The $x_{(k)}$ sample element is considered to be the estimated noise level, which is then multiplied by a threshold factor T (often predefined by the user) in order to obtain the final threshold value Z for the radar return in the CUT per time. The comparator then compares x_0 with Z to output a final decision, which can be any of two outcomes: if $x_0 > Z$, then a target return is detected in the CUT, however, if $x_0 \leq Z$, then no target is detected in the CUT except noise.

Following the above description of the DA-OS scheme, it is noted that the choice of the kth rank ordered element determines how accurate the noise estimate will be, thus determining the performance level of the OS scheme. Consequently, our aim is to construct an algorithm that can accurately and automatically

estimate the kth rank ordered element of the OS scheme without *a priori* knowledge of the characteristics (i.e. distribution) of the input radar returns. We discuss such an algorithm in the next subsection.

3.2. The DA-OS algorithm

The DA-OS algorithm is motivated following the performance of the well-known Otsu's method deployed for binary image segmentation in many image processing applications [31]. Here, similar to the approach used in the Otsu's method, we construct an effective algorithm deployable for target detection in radar systems for remote sensing applications. To the best of our understanding, such an approach has not been explored for radar systems prior to the present study.

Essentially, the principle of discriminant analysis used in Otsu's method aims to compute the between-class variance (BCV) value for every pixel in the histogram of an input image [31]. It has also been applied in cognitive radio applications [32,33]. The BCV is a measure of the degree of separation between two classes. To compute this measure as deployed in Otsu's method, the histogram of an input grey-scale image is first generated, and each bin of the histogram is used to bifurcate the image into two classes, i.e. the foreground and background pixels. Then, the BCV value corresponding to each bin is computed, and the bin (i.e. the pixel value) with the highest BCV value is selected to be the optimal threshold value for effective image segmentation.

Following the above explanation, in the present article, we note that since the BCV value is capable of measuring the degree of separation between two classes of an input sample generated from the same dataset (for example, an image in the case of Otsu's method), consequently, such a measure can as well be applied to measure the degree of homogeneity/non-homogeneity in the case of radar systems. Thus, following Otsu's method in [31], our idea postulates that if the measured input radar returns comprise noise-only elements (i.e. in the homogeneous condition), then the computed BCV value per sample will be quite small since the difference between the mean of any two classes formed in this case will be zero (or approximately zero). On the other hand, if the measured returns in the reference windows contain some signal components, then the BCV value will be large since one of both classes will contain signal elements, and thus the difference between the means of any two classes from the set of radar returns will be large, which indicates a non-homogeneous condition.

Consequently, we constructed the DA-OS algorithm in order to test the validity of the above hypothesis towards improving the performance of the known OS scheme and results in this regard are discussed in Section 5. The input to the DA-OS algorithm is the ordered sample $X_{(N)} = \{x_{(1)}, x_{(2)}, x_{(3)}, \ldots, x_{(N)}\}$ obtained from both the leading and lagging cells of the reference window. The aim of the DA-OS algorithm is to compute the BCV value of each element located in the CUT at any point in time, particularly as the CUT sweeps through the reference window. Thus, the algorithm computes the BCV of each element n in the CUT by averaging the BCV values computed for all other cells in the reference window. Hence, in order to compute the BCV value of each nth element located in the CUT, we initiated an index $m = 1, 2, 3, \ldots, N$ used to indicate the BCV values of all other elements in the reference window. Thus, for each mth index, the elements in the reference window are first bifurcated into two classes X^L and X^U, where $X^L = \{x_{(1)}, x_{(2)}, \ldots, x_{(m)}\}$, and $X^U = \{x_{(m+1)}, x_{(m+2)}, \ldots, x_{(N)}\}$, and the entire input sample $X_{(N)}$ is then $X_{(N)} = \{X^L, X^U\}$. Then, the algorithm computes the means μ_m^L and μ_m^U of X^L and X^U, respectively, for $m = 1, 2, 3, \ldots, N$ as follows:

$$\mu_m^L = \frac{1}{m}\sum_{n=1}^{m} x_{(n)}, \tag{1}$$

$$\mu_m^U = \begin{cases} \dfrac{1}{N-m}\displaystyle\sum_{n=m+1}^{N} x_{(n)}, & \text{if } m < N \\ 0, & \text{if } m = N \end{cases} \tag{2}$$

and the probabilities per mth index p_m^L and p_m^U of X^L and X^U, respectively, are computed as follows:

$$p_m^L = \frac{m}{N}, \tag{3}$$

$$p_m^U = \begin{cases} 1 - p_m^L, & \text{if } m < N \\ 0, & \text{if } m = N. \end{cases} \tag{4}$$

Note that for $m = N$, only one class exists, i.e. the X^L class, and thus the mean μ^U and the corresponding probability p^U of X^U in this case will be zero, as indicated in Eqs. (2) and (4), respectively. Thus, the DA-OS algorithm proceeds to compute the BCV value F of each mth index as [31]

$$F_m = p_m^L \cdot p_m^U \left[\mu_m^L - \mu_m^U\right]^2, \text{ for } m = 1, 2, 3, \ldots, N. \tag{5}$$

Consequently, the algorithm computes the mean of F_m to be the average BCV value of each nth element located in the CUT per time as follow

$$\overline{F}_n = \frac{1}{N}\sum_{m=1}^{N} F_m, \text{ for } n = 1, 2, 3, \ldots, N. \tag{6}$$

Eq. (6) reveals that $\overline{F}_n$ is computed for each element n in the reference window as the CUT sweeps across each cell in the reference window. Therefore, $\overline{F}_n$ is a stable metric for measuring the degree of homogeneity in the reference window because the BCV value of all elements in the reference window (see Eq. (5)) are averaged towards computing the BCV value of the element in the CUT. Thus, the variance of the BCV values in Eq. (5) is greatly reduced by the averaging process in Eq. (6). This provides the DA-OS algorithm with an intuitive mechanism for determining the actual number of interfering targets K as well as clutter edges present in the reference window, particularly as the CUT sweeps across each element in the reference window. Thus, K is determined as follows:

$$K = \begin{cases} 0, & \text{if } \overline{F}_n < \theta \\ K + 1, & \text{if } \overline{F}_n - \overline{F}_{n-1} > \theta \text{ and } K < \frac{N}{2} - 1. \end{cases} \tag{7}$$

where θ is a threshold value used to determine whether the reference window contains homogeneous elements or not. Essentially, θ can be assigned a small value, typically $\theta = 0.5$ as in our experiments since homogeneous radar returns in the reference window will always produce very small $\overline{F}_n$ values. The choice of $\theta = 0.5$ is further valid since for a homogeneous reference window, i.e. when $\mu^L \approx \mu^U$, we obtain $F_m \approx 0$, which could be made equal to zero by applying a flooring function. Nevertheless, since a flooring function was not used, we consider $\theta = 0.5$ as a valid threshold value across a wide range of conditions as will be shown in the graphical results of Section 5.1.

In order to apply Eq. (7) effectively, the DA-OS algorithm initializes K as $K = 0$ and $\overline{F}_{n-1}$ as $\overline{F}_{n-1} = 0$. These initial values are assumed to be valid since the scheme cannot determine whether or not an interfering signal is present in the reference window until the content of the first cell in the CUT is processed. However, these parameters are subsequently updated by the algorithm after each cell in the CUT is processed (see step 14 of Algorithm 1). Furthermore, the condition $K < \frac{N}{2} - 1$ is introduced in Eq. (7) in order to ensure that K is not incremented beyond half of the reference window size. This measure prevents the DA-OS scheme from incurring high false alarm rates at clutter edges since only clutter returns are able to occupy the entire half of any reference window [16].

Thus, since the elements in the reference window are ordered, then the kth rank ordered element for the DA-OS scheme can be obtained easily as

$$k = N - K \tag{8}$$

By using Eq. (8) to obtain the kth rank ordered element of the OS scheme, the DA-OS algorithm can then easily output $x_{(k)}$ as the final estimate of the noise level in the reference window, which will be multiplied by the threshold factor T (as in Fig. 1) towards obtaining the final threshold value Z, which reads

$$Z = T \times x_{(k)} \tag{9}$$

where the value of T was computed via Monte Carlo simulation. To determine T, random samples of additive white Gaussian noise elements (i.e the homogeneous condition) were generated during each Monte Carlo trial and then the value of T was successively varied and applied per CFAR scheme and their resulting P_{FA} values were computed using Eq. (11). The P_{FA} results obtained as a function of T is plotted as discussed in Section 5.2.1 and then the appropriate choice of T that corresponds to a desired P_{FA} rate was selected per CFAR scheme. Further, a summary of the entire algorithmic procedure to execute the DA-OS scheme is presented in Algorithm 1.

3.3. Time complexity analysis

In order to analyse the time complexity (TC) of the DA-OS algorithm, we considered the number of machine instructions required to execute the algorithm as a basis for approximating the TC. To achieve this, we excluded all constant factors within the steps of the DA-OS algorithm in order to ensure that its running time scales only according to the input sample size N, particularly as N tends to infinity. Similarly, we excluded lower order terms in order to asymptotically describe the TC [34]. Thus, Eqs. (1)–(5) can be considered to be evaluated in constant time only once in steps 5–7, which reduces to a TC of $\mathcal{O}(1)$ per step. The reordering process of the input radar returns in the reference window can be achieved within a TC of $\mathcal{O}(N)$, particularly by using some of the best sorting algorithms, for example, the Timsort algorithm [35]. Since there are two nested *for* loops between steps 3–21 of Algorithm 1, we obtain in this case an asymptotic TC of $\mathcal{O}(N^2)$. Thus, by neglecting lower order terms, the approximate overall TC of the DA-OS algorithm for the CUT sweeping through the entire reference window is given as $TC \approx \mathcal{O}(N^2)$. However, the approximate TC for computing the threshold value of a single cell located in the CUT is $TC \approx \mathcal{O}(N)$ since only the *for* loop between steps 4–11 will be considered in this case. The TC of the DA-OS algorithm is compared with other well-known CFAR algorithms in Table 1. There, it can be seen that the DA-OS algorithm suffices as a more complex algorithm, and thus slower as against the CA, SOCA, GOCA, and OS schemes. However, we shall show in Section 5 that although complex, the DA-OS scheme offers better detection, as well as lower false alarm rates as against other basic schemes, particularly under conditions of non-homogeneous radar returns.

Algorithm 1: DA-OS Algorithm

Input:

1. Ordered radar returns in the reference window: $X_{(N)} = \{x_{(1)}, x_{(2)}, ..., x_{(N)}\}$, where $x_{(1)} < x_{(2)} < x_{(3)} < ... < x_{(N)}$;
2. BCV Threshold: $\theta = 0.5$;
3. Reference window size: N;
4. Threshold factor: T_{DA}

Output:

1. Number of interfering targets: K;
2. kth rank ordered element: k;
3. Threshold value: Z

// Initialize variables
1 $K \leftarrow 0$;
2 $\overline{F}_{n-1} \leftarrow 0$;
// The BCV will be computed for each cell n located in the CUT as the CUT sweeps through each cell in the reference window
3 **for** $n = 1$ *to* N, **do**
4 **for** $m = 1$ *to* N, **do**
5 Compute μ^L and μ^U using Eqs. (1) and (2), respectively;
6 Compute p^L and p^U using Eqs. (3) and (4), respectively;
7 Compute $F_{(m)}$ using Eq. (5);
8 **if** $m == N$ **then**
9 $\mu^U = 0$, $p^U = 0$, $F_{(m)} = 0$;
10 **end**
11 **end**
12 Compute $\overline{F}_n$ using Eq. (6);
13 **if** $\overline{F}_n - \overline{F}_{n-1} > \theta$ & $K < \frac{N}{2} - 1$ **then**
14 $K = K + 1$; *Update the number of interfering targets in the reference window*
15 **else**
16 $K = 0$; *No interferer was detected (i.e. homogeneous condition detected)*
17 **end**
18 $\overline{F}_{n-1} \leftarrow \overline{F}_n$; *Update the average BCV for the next CUT*
19 $k = N - K$; *Obtain the kth rank ordered element*
20 $Z_n = T_{DA} \cdot x_{(k)}$; *Obtain threshold value for the present CUT*
21 **end**
22 Return k, K, Z_n

Table 1
Asymptotic Time Complexity of the different CFAR schemes.

	CFAR SCHEMES				
	CA	SOCA	GOCA	OS	DA-OS
Asymptotic Time Complexity	$\mathcal{O}(N)$	$\mathcal{O}(N)$	$\mathcal{O}(N)$	$\mathcal{O}(N)$	$\mathcal{O}(N^2)$

4. Method of simulation and analysis

4.1. Simulation

A monostatic radar system was assumed in our simulation since a single antenna was considered in our design as shown in Fig. 1. All transmission parameters leading to the simulated received returns were assumed to be appropriately designed, thus guaranteeing that the range gates of the radar system were opened accurately according to the pulse repetition frequency (PRF). Consequently, we present simulated traces in Section 5 representing radar returns at different range cell indexes. Furthermore, we considered the case for non-coherent integration in our design because it reduces the very high and impractical transmit power levels (SNR $\approx$ 15–35 dB) often required to achieve high detection rates (P_d > 90%) as in the case of single pulse transmission. In this regard, a number of pulses N_P were considered in our simulation of the non-coherent video integration process. These pulses were averaged per range cell in order to obtain the final traces shown in the different graphs of Section 5.

We simulated conditions of homogeneous noise-only radar returns using random elements drawn from a complex additive white Gaussian noise (AWGN) model $X \sim \mathcal{CN}(0, \sigma^2)$ of zero-mean and unit variance $\sigma^2 = 1$. For non-homogeneous target returns, the Swerling II model was used to simulate the target returns considered to be simple point scatterers fluctuating between pulses but constant in a single scan. Consequently, all targets in the CUT as well as other interfering targets were simulated according to the Swerling II model. Clutter returns were modelled as a series of single targets occupying a set of contiguous range cells.

Having established the noise, target, interferer, and clutter models using complex AWGN and Swerling II models, respectively, and in the absence of tractable mathematical analysis of the BCV statistics, we used Monte Carlo simulation to conduct and analyse the performance of the different schemes as follows:

1. Let the total number of Monte Carlo trials be C, indexed as $c = 1, 2, \ldots, C$
2. N_P pulses were generated using the different models for the different radar environments, and averaged to obtain the final received radar returns $X_N = \{x_1, x_2, x_3, \ldots, x_N\}$ per environment, where N refers to the reference window size.
3. The different CFAR schemes were subjected to X_N according to their respective working principles, including the DA-OS scheme. Recall that for the fixed OS and DA-OS schemes, X_N will be ordered as $X_{(N)}$ prior to further processing, whereas the unordered sample X_N will be processed in the CA, SOCA, and GOCA schemes, which do not require any pre-ordering process.
4. The series of estimated threshold values Z_n obtained via the different techniques were then compared to X_N.
5. The probability of detection P_d and probability of false alarm P_{fa} were computed per trial c, to be described in the next subsection.
6. The process was repeated C times and averaged to obtain the average P_d and P_{fa} values against different SNR values as well as against different clutter cell positions as reported in Section 5.

4.2. Analysis

In order to analyse the different CFAR schemes, the elements comprising a single sample of radar returns $X_N = \{x_1, x_2, x_3, \ldots, x_N\}$ located in the reference window were compared against their corresponding threshold values $Z_N = \{z_1, z_2, z_3, \ldots, z_N\}$ estimated per Monte Carlo trial $c = 1, 2, 3, \ldots, C$. Then, the P_d and P_{fa} of each technique were computed respectively as follows:

$$P_d = \frac{1}{C \times N} \sum_{c=1}^{C} \sum_{n=1}^{N} D_{c,n} \tag{10}$$

$$P_{fa} = \frac{1}{C \times N} \sum_{c=1}^{C} \sum_{n=1}^{N} F_{c,n} \tag{11}$$

where,

$$D_{c,n} = \begin{cases} 1, & \text{if } x_{c,n} > z_{c,n}, \text{ given that } G_{c,n} = 1, \\ & \text{for } n = 1, 2, 3, \ldots, N; \quad c = 1, 2, 3, \ldots, C \\ 0, & \text{if otherwise} \end{cases} \tag{12}$$

and

$$F_{c,n} = \begin{cases} 1, & \text{if } x_{c,n} \geq z_{c,n}, \text{ given that } G_{c,n} = 0, \\ & \text{for } n = 1, 2, 3, \ldots, N; \quad c = 1, 2, 3, \ldots, C \\ 0, & \text{if otherwise} \end{cases} \tag{13}$$

Table 2
Simulation parameters and their respective values.

Parameter	Values
Total number of Monte Carlo trials, C	10^3
Number of pulses, N_P	10
Reference window size, N	16
kth element of the fixed OS scheme	12

where we recall that $x_{c,n}$ refers to the value of a single radar return located in a single cell index n per Monte Carlo trial c, whereas $z_{c,n}$ refers to the corresponding threshold value estimated for the same cell index n per trial c. $G_{c,n}$ denotes the binary ground-truth dataset comprising zeros and ones, where $G_{c,n} = 1$ indicates that a signal truly exists in the CUT n per trial c, whereas $G_{c,n} = 0$ signifies that in truth no signal exists in the CUT except noise. It is noted that $G_{c,n}$ is created *a priori* in order to compute accurately the values of P_d and P_{fa}.

5. Results and discussion

The DA-OS algorithm was evaluated and compared against other known schemes such as the CA, SOCA, GOCA and OS schemes. In this section, first, we present and discuss results to illustrate the dynamics of the BCV value. Then, we discuss results obtained under conditions of homogeneous and non-homogeneous environments. Table 2 highlights the parameters and their respective values as considered in the Monte Carlo simulation. The kth element of the fixed OS scheme, without any automatic censoring procedure, was obtained using the optimum criterion of $k = \frac{3}{4}N$ [22]. All codes and simulations were conducted in MATLAB R2019a.

5.1. Adaptivity of the proposed method

This subsection presents and discusses results to demonstrate the adaptiveness of our proposed method based on the BCV value. In this regard, we considered three different radar operating environments, which included single targets located in homogeneous noise radar returns, multiple interfering targets within the reference window, and radar returns situated at different clutter power levels. For each condition, we ensured that a predefined $P_{fa} = 10^{-3}$ rate was maintained for a window size of $N = 16$. Consequently, an estimated threshold factor of $T_{DA\_OS} = T_{OS} = 2.72$ was used and maintained across each operating condition for our proposed method and the fixed OS(12) scheme, respectively. In the following subsections, we illustrate and discuss how the estimated BCV value would typically adapt under different operating environments in order to estimate accurately the kth rank ordered element of the OS scheme. Our findings are presented as follows:

5.1.1. Under single target in homogeneous return

Here, we discuss results that illustrate how our proposed method operates in the presence of a single target within a reference window comprised of homogeneous noise-only radar returns. First, Fig. 2(a) displays the simulated target returns located at the 10th, 40th, and 80th range cells, respectively, while other cells simply contained noise-only radar returns. Although simulated, nevertheless, under real-life conditions, these target returns could correspond to echoes emanating from objects located within the operating space of a mobile industrial robot, i.e. in the case of object detection, or they may belong to echoes emanating from an intruder(s) lurking within an industrial environment in the case of measurements from a security monitoring device. More generally, they could emanate from a wide range

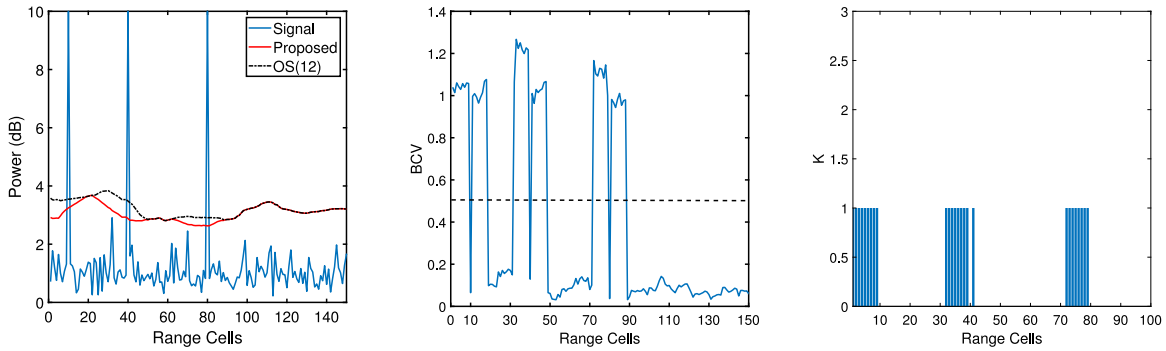

Fig. 2. Estimated BCV and kth rank ordered value under single target returns in homogeneous radar returns.

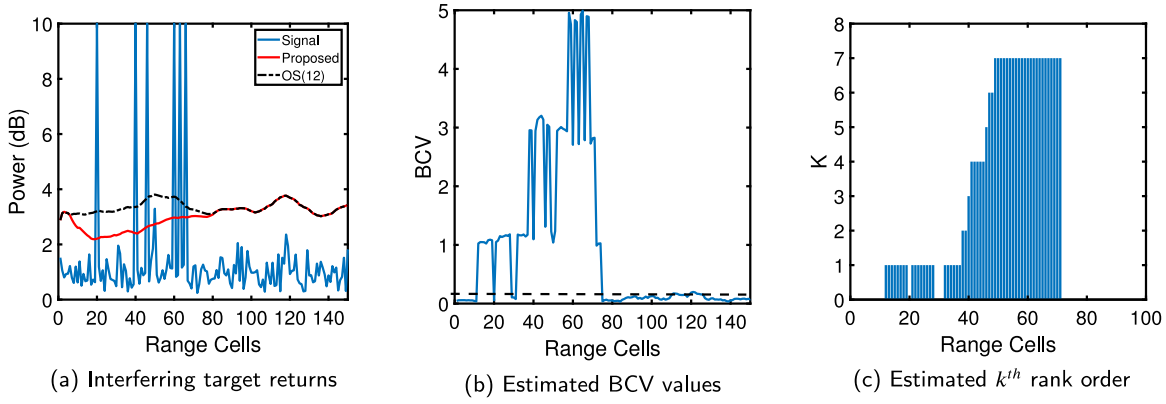

Fig. 3. Estimated BCV and kth rank ordered value under multiple interfering targets radar returns.

of application areas, which are not limited only to the above-mentioned examples. By using a window size of $N = 16$, we ensured that only one target return was captured within the reference window during the entire simulation period since these targets were well separated in the range cells (i.e separated by more than 16 range cells) as seen in Fig. 2(a).

Fig. 2(b) displays the BCV value computed by our method over the entire swept range cells. Essentially, if a high BCV value is computed at any range cell, it typically implies that there exists non-homogeneous radar return(s) within the reference window at that point in time, whereas, if a low BCV value (below the threshold line) is computed at any range cell, then it implies that all elements within the reference window at that point in time are homogeneous in nature (i.e. they are elements of equal average power level). Thus, following Fig. 2(b), a relatively high BCV value of about 1 was computed for the 1st range cell up until the 10th cell because the first target return located at the 10th cell was situated within the reference window, thus confirming the presence of a non-homogeneous element (i.e. the target return) at the 10th cell. Consequently, it can be explained easily that the low BCV value computed at the 10th cell occurred because the radar return in the 10th cell was expunged for being in the CUT at that point in time, thus leaving only noise radar returns (i.e. homogeneous elements) within the reference window, thus leading to the low BCV value computed at that point in time. However, as soon as the CUT progressed to the 11th cell, it is seen that the BCV value immediately increased above the threshold line because at that point, the target return was once again situated in the leading cells of the reference window. Nevertheless, as the reference window progressed beyond the 16th cell, the BCV value again dropped towards zero since the target return had completely progressed out of the reference window, thus leaving only homogeneous noise-only returns within the reference window.

Further, Fig. 2(b) shows that the above process for the computed BCV value was repeated for the second target, starting from the 32nd cell where the BCV value increased above the threshold line. As expected, the BCV value dropped rapidly towards zero at the 40th cell since the target return was now in the CUT and thus expunged from the reference window. The process correctly repeated itself for the third target located at the 80th cell. Here, we observed that the BCV value rose at the 72nd cell above the threshold line, and then dropped below the threshold line at the 88th cell because at that point, the target cell was now completely out of the reference window. Thereafter, a low BCV value, way below the threshold line, was computed for the cells beyond the 88th range cell, thus indicating that no target return existed in the reference window after the 88th cell.

Consequently, following the deterministic behaviour of the BCV value, Fig. 2(c) shows that our method accurately estimated the presence of a single target return (i.e $K = 1$) within the reference window at the relevant range cells. Here, K represents the total number of targets within the reference window, thus implying that the kth element was $N - K$, i.e the 15th element in our case for $N = 16$. Hence, by accurately estimating the kth element for the OS scheme, our method selected the OS(15) scheme for use. Thus, Fig. 2(a) displays the adaptive threshold values computed based on our method along with the threshold values estimated using the OS(12) scheme (i.e based on the kth $=$ 12 element). Under both configurations, the three targets were successfully detected thus implying that our method performed equally as well as the OS(12) scheme under the tested condition. We note that the estimated K values in Fig. 2(c) are similar because our algorithm was able to detect the single targets that were present in the reference window per time. The energy of the targets in Fig. 2(a) were set to the same value, however, it

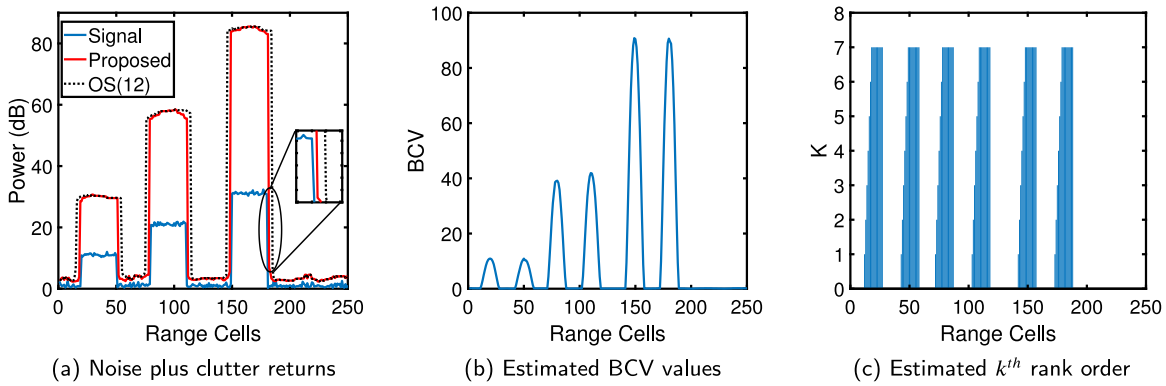

(a) Noise plus clutter returns (b) Estimated BCV values (c) Estimated k^{th} rank order

Fig. 4. Estimated BCV and kth rank ordered value under different clutter power levels.

can be observed that they were well separated in the range cells. Thus, this ensured that only one target appeared per time in the reference window during the entire simulation process, thus resulting in the same K value as obtained in Fig. 2(c).

5.1.2. Under conditions of multiple interfering targets

We simulated the presence of multiple targets as shown in Fig. 3(a) with targets located at the 20th, 40th, 46th, 50th, 60th, 63rd, and 66th range cells. A reference window size of $N = 16$ was maintained, which ensured that the 40th, 46th, and 50th targets were all within the reference window at the same time. This created the presence of three targets in the reference window when the CUT was situated at the 42nd range cell. Also, when the CUT was situated at the 58th cell, then the 60th, 63rd, and 66th targets were all captured within the reference window at the same time.

Following Fig. 3(b), it can be observed that when the CUT was at the 12th cell, then the first target located at the 20th range cell drifted into the reference window, which accounted for the high BCV value estimated from the 12th cell and onward. As expected, the estimated BCV value dropped rapidly at the 20th cell since the target in the 20th cell was expunged for being in the CUT at that point in time. The BCV value increased rapidly afterwards because the target in the 20th cell reappeared in the leading cells of the reference window.

An interesting observation can be noted at the 32nd range cell when the target at the 40th cell drifted into the reference window. At that point, Fig. 3(b) shows that the BCV value increased to an average value of 1. However, this value soon increased again at the 38th cell because the next target at the 46th cell drifted into the reference window, thus further increasing the computed BCV value owing to the presence of the two targets within the reference window at that point in time. Notice that the BCV value dropped at the 40th cell since it was expunged for being in the CUT. However, we observed that the BCV value did not drop below the threshold line as expected because although the 40th target may have been expunged, nevertheless, the target at the 46th cell was still within the reference window, thus preventing the BCV value from dropping way down to zero. Similarly, the BCV value further increased at the 58th cell because the target at the 50th cell, as well as the targets at the 60th, 63rd, and 66th cells were all captured within the reference window at the same time. This accounted for the four targets being situated in the reference window at that point in time. Essentially, the BCV value increased accordingly to account for each target within the reference window. Close observation of Fig. 3(b) indicates that the BCV value dropped at each target location since each target was expunged from the reference window when they were in the CUT. Consequently, the trace of the BCV values in Fig. 3(a) dropped below the threshold line after the 74th range cell because all the targets were now completely out of the reference window. The BCV value remained very low onward from the 74th range cell, which correctly indicated that no target existed beyond the 74th cell.

Following the above dynamics of the BCV value, Fig. 3(c) displays the estimated number of targets K within the reference window throughout the simulation period at each range cell. The kth rank ordered element was then effectively calculated at each point as $N - K$, which enabled our scheme to accurately estimate the adaptive threshold value for each range cell as shown in Fig. 3(a). We note from Fig. 3(c) that our method correctly estimated the presence of 7 targets, which tallied correctly with the actual number of targets displayed in Fig. 3(a). Furthermore, our method demonstrates its superiority as against the OS(12) scheme by adapting effectively to detect the low SNR target located at the 50th range cell. The fixed OS(12) scheme failed in this regard since it lacked the capability to effectively adapt the kth rank ordered in order to improve the performance of the OS scheme under these dynamic non-homogeneous conditions.

5.1.3. Under conditions of different clutter power levels

We considered different clutter power levels within the reference window as shown in Fig. 4(a). The first clutter occurred between the 10th–50th range cells at an average clutter-to-noise ratio (CNR) of 10 dB The second clutter was situated between the 80th–110th range cells at an average CNR of 20 dB, whereas the third clutter appeared between the 150th–180th range cells at an average CNR of 30 dB.

Fig. 4(b) presents the estimated BCV values as the reference window swept across the entire range cells. Since the clutter edges were sharp and abrupt in nature, we observed that the BCV values increased and decreased smoothly across the edges of each clutter range. However, the BCV value did not drop rapidly at the clutter edges as initially expected (see Sections 5.1.1 and 5.1.2, respectively), since when the clutter edges were in the CUT, the entire lagging cells of the reference window were entirely occupied by clutter returns, thus producing a very high BCV value at that point in time. Consequently, we note that the BCV value was maximum at the sharp clutter edges when these edges were in the CUT, i.e. at the clutter boundaries (the 10th, 50th, 80th, 110th, 150th, and 180th range cells). However, when the reference window drifted beyond the clutter edges, the BCV value slowly dropped towards zero since after each edge, the radar returns were comprised only of homogeneous noise elements (i.e. at the plateau of each clutter level). Fig. 4(b) shows clearly that the BCV value increased further at each rising edge according to the power level of each clutter level, which accurately affirms that each succeeding clutter range was more powerful than the preceding one.

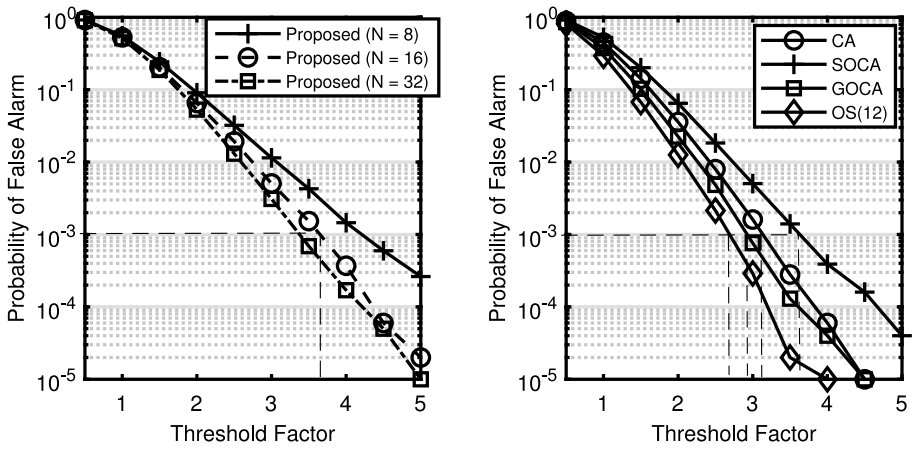

(a) Proposed Technique under different reference cell sizes (b) Other techniques under reference cell size N = 16

Fig. 5. Probability of false alarm versus Threshold factor to determine the appropriate threshold factor to be used per technique.

Following the dynamics of the estimated BCV value in the clutter case of Fig. 4(b), our proposed method is shown in Fig. 4(c) to have progressively estimated the number of targets as 7 at each clutter edge. The number of targets was halted at 7 in order to prevent an excessive false alarm rate from occurring at the clutter edges, since it implies that the entire lagging cells of the reference window (i.e $\frac{N}{2} - 1$) were totally occupied by clutter returns. Thus, the use of the effective BCV value by our method presents any radar system or an operator with a dependable metric to automatically determine the actual number of targets and clutter edges within a reference window, as well as to provide an idea of their respective signal strengths. This implies that the BCV value is an effective deterministic metric for measuring the degree of homogeneity/non-homogeneity of radar returns within a reference window. Specifically, when the BCV value is close to zero (i.e. below the threshold line of 0.5), then the returns are homogeneous in nature (noise-only returns), whereas when the BCV value is above the threshold line, then there exists non-homogeneous returns (presence of targets/clutter edges) in the reference window. Following this mechanism, we have demonstrated that our method adapts effectively to the different operating conditions in which radar systems are expected to be deployed.

The case of detecting multiple clutters in a single reference window can be achieved by observing that the BCV trace of Fig. 4(b) rises and falls in a consistent pattern at clutter edges. Thus, the DA-OS algorithm can be modified to monitor the gradients of these rise-fall patterns in order to detect the potential presence of full clutter ranges in a reference window. However, such a modification was not considered in the present article since we used only a small and realistic window size of N = 16, which may not be large enough to accommodate the full range of a typical clutter.

5.2. Homogeneous environment

In this subsection, we discuss results pertaining to the selection of the threshold factor used in our method, as well as in the CA, SOCA, GOCA and OS(12) schemes, towards maintaining $P_{fa} = 10^{-3}$ based on a reference window size of $N = 16$. Then, using these established threshold factors, we determined the minimum SNR performance of our method compared with the CA, SOCA, and GOCA schemes under the condition of homogeneous noise-only radar returns containing a single target in the CUT without interfering targets.

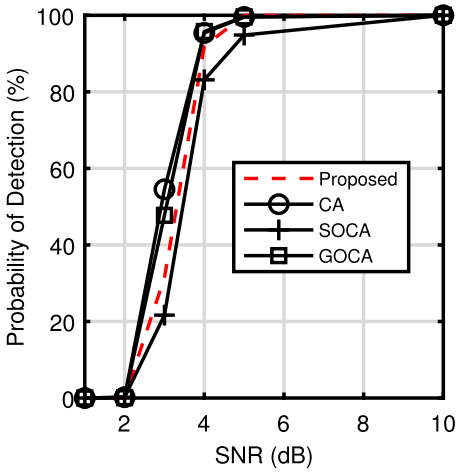

Fig. 6. Probability of Detection versus SNR (under homogeneous noise condition containing a single target (No interfering targets) for N = 16, $P_{fa} = 10^{-3}$).

5.2.1. Performance under noise-only radar returns

In order to obtain the threshold factors that would maintain $P_{fa} = 10^{-3}$, first, we examined our method under different reference window sizes under the condition of homogeneous noise-only radar returns. Monte Carlo simulation was again performed to obtain the results presented in Fig. 5(a).

As expected, Fig. 5(a) shows that the P_{fa} rate decreases with an increase in the threshold factor for the different reference window sizes considered in our experiments. This result agrees with theory as well as with classic results in the literature [16,18] since an increase in the threshold factor typically corresponds to an increase in the actual estimated threshold value, which invariably reduces the P_{fa} rate of our scheme. We note that only the P_{fa} rate is reported in this case since only noise radar returns were considered in this experiment. Furthermore, the P_{fa} rate also decreased with an increase in N, which agrees with theory as well as with known results in the literature [16,18]. The choice of a reference window size of $N = 16$ is often used in the literature as a fair balance between reducing computational complexities (i.e. efficiency) as well as maintaining the accuracy of detection (i.e. effectiveness). Consequently, we considered $N = 16$ in all our experiments, and Fig. 5(a) shows that a threshold factor of $T_{DA\_OS} = 3.67$ was obtained in order to maintain $P_{fa} = 10^{-3}$.

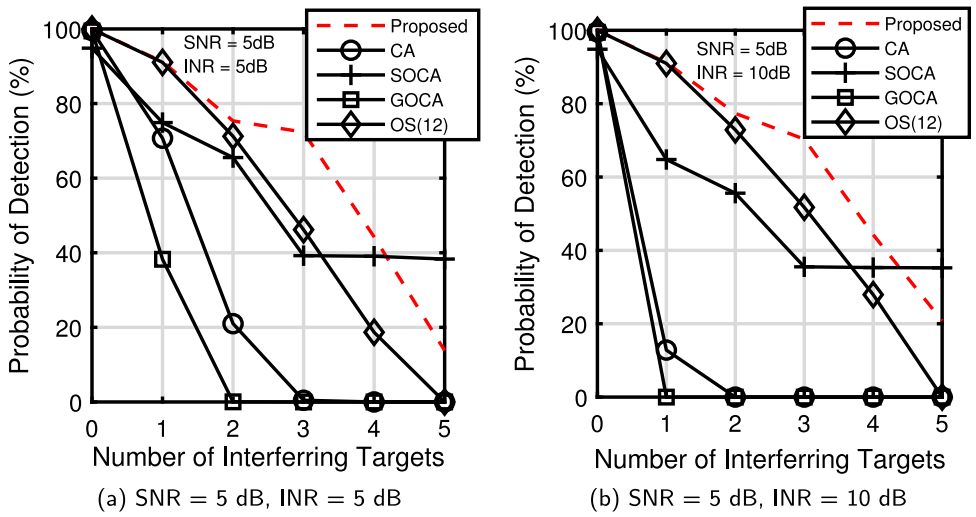

Fig. 7. Probability of Detection versus the number of Interfering targets in the lagging cells of the reference window at different INRs for N = 16, $P_{fa} = 10^{-3}$.

This threshold factor was thus maintained for our method in succeeding experiments reported hereafter.

The CA, SOCA, GOCA and OS(12) schemes were examined as well, and results obtained are presented in Fig. 5(b). In this case, a reference window size of $N = 16$ was maintained. Fig. 5(b) shows that the following threshold factors were obtained to maintain $P_{fa} = 10^{-3}$ for each technique as follows: $T_{ca} = 3.06$, $T_{soca} = 3.696$, $T_{goca} = 2.876$, and $T_{OS} = 2.575$, respectively. Except stated otherwise, these values were maintained throughout other experiments reported in this subsection.

5.2.2. Performance under single target in homogeneous noise-only radar returns

Having established the required threshold factors for each technique under the condition of homogeneous noise-only radar returns, we then examined the SNR performance of our method compared with the CA, SOCA, and GOCA schemes under the condition of a single target in noise homogeneous conditions. The results obtained are reported in Fig. 6. In Fig. 6, we show that our proposed technique performs closely with the classic CA method under conditions of homogeneous noise radar returns with a single target. For the case of non-coherent detection, we note that our method achieves $\approx$ 100% detection rate at an approximate SNR level of 5 dB. Further, since the CA is considered to be the optimum scheme under the homogeneous noise condition with a single target, thus, we report in Table 3 the CFAR loss of each method with reference to the CA scheme at $P_d = 0.5$. Here, our proposed method presents a small CFAR loss of 0.392 dB at $P_d = 0.5$. The GOCA and SOCA schemes provided a CFAR loss of about 0.121 and 0.512 dB with respect to the CA technique, respectively, which agrees closely with reported values in the classic literature [16,18]. Essentially, with such a small CFAR loss as a benchmark, it is argued that our proposed method provides a considerably high detection performance rate for the case of detecting single targets under the condition of homogeneous noise-only radar returns within the reference window. In the next subsection, we shall present results obtained for the case of a more challenging condition comprising non-homogeneous radar returns within the reference window.

5.3. Non-homogeneous environment

In this subsection, first, we discuss the performance of our method against other techniques under different non-homogeneous conditions comprised of multiple interfering targets within the reference window at different interference-to-noise-ratio (INR) levels. In the subsequent subsection, we examine an encompassing as well as challenging dataset comprised of all conditions including homogeneous noise-only conditions, single target, multiple targets, and clutter edges, and clutter-plus-interference conditions. The results obtained are discussed as follows:

Table 3
CFAR loss (in dB) of the different methods with respect to the CA at $P_d = 50\%$, $P_{fa} = 10^{-3}$, $N = 16$.

Method	SNR (dB)	Loss (dB)
CA	2.926	–
SOCA	3.438	0.512
GOCA	3.047	0.121
Proposed	3.318	0.392

5.3.1. Detection performance under multiple interfering targets in noise only radar returns

Fig. 7 presents the detection performance of the different methods as a function of the number of interfering targets N_I within a reference window size of $N = 16$. In this case, we considered the case when the INR of the interfering target is same with the target return in the CUT (see Fig. 7(a)), as well as the case of doubling the INR value in Fig. 7(b). Following several Monte Carlo simulations, it was noted that the detection performance of each method decreased as the number of interfering targets increased within the lagging cells of the reference window. This report is consistent with classic and theoretical results obtained in the literature [16,18]. Particularly, the GOCA and CA schemes were the least performers, whereas our method outperformed both the OS(12) and SOCA schemes over the tested range. The result of Fig. 7(a) indicates that it is often impossible for the GOCA and CA schemes to detect the target signal in the CUT when $N_I > 3$. This observation is valid since both the CA and GOCA schemes are prone to the effect of target masking in the presence of interfering targets. On the other hand, the OS(12) scheme maintains some detection capability until $N_I > 4$. This observation is again correct since the performance of the OS(12) scheme can only be guaranteed so long as the kth element, in this case the 12th element, is not exceeded. However, we show that our proposed method effectively adapts the value of the kth element in order to correctly track the actual number of

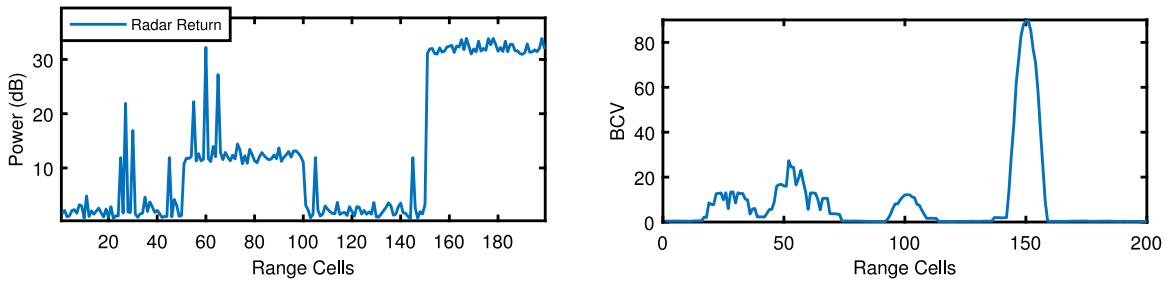

(a) Radar returns over the range cells (b) BCV values over the entire range cells

Fig. 8. Simulated range cells containing radar returns from a complex environment and the corresponding BCV trace.

Table 4
Description of the radar returns in the range cells of Fig. 8(a).

Range cells	Description
1–24, 31–44, 46–50, 106–144, 146–150	Noise-only radar returns
25, 27, 30, 45, 105, and 145	Targets at 10 dB, 20 dB, 15 dB, 10 dB, 10 dB, and 10 dB, respectively
51–100, 151–200	Noise plus clutter ranges at 10 dB and 30 dB, respectively
55, 60, and 65	Noise, clutter plus target returns at 20 dB, 30 dB and 25 dB, respectively

interfering targets present in the reference window. Thus, this led to a generally better performance than the OS(12) scheme and other schemes. It should be noted that the performance of the SOCA scheme may have outperformed our DA-OS scheme at $N_l > 5$ simply because the interfering targets were situated in only one half of the reference window (i.e in the lagging cells). It is well known that the performance of the SOCA scheme typically degrades similarly to the CA scheme whenever the interfering targets are situated concurrently in both the leading and lagging cells of the reference window [18].

Further, we noticed only a little change in the performance of our method, the OS(12), and the SOCA schemes, particularly when we doubled the INR value as in Fig. 7(b). The invariance of our method to an increase in the INR values is explained based on the fact that our method is always able to accurately detect and censor the interfering targets within the reference window. Consequently, despite increasing the INR values, our method was able to accurately censor the interfering targets, thus eliminating their effect on the estimated threshold value. Hence, by expunging the interfering targets from the reference window, our DA-OS scheme was able to maintain a high P_d performance rate. On the other hand, it can be seen that the CA and GOCA methods were grossly affected by an increase in the INR value. Their performance was grossly degraded because both methods were unable to expunge the interfering targets in the reference window prior to threshold computation. Thus, an increase in the INR values of the interfering targets apparently led to an increase in the threshold values estimated by the CA and GOCA methods, which consequently led to a poorer P_d performance.

5.3.2. Detection performance under target, noise and clutter radar returns

Fig. 8(a) presents the radar returns of a highly complex non-homogeneous environment comprising multiple targets of varying INR levels, rising and falling clutter edges, as well as multiple targets plus clutter returns. The radar returns and the corresponding threshold values estimated per technique were averaged over 1000 Monte Carlo simulations in order to improve the statistical significance of the obtained results. The contents of the range cells of Fig. 8(a) are described in Table 4.

In the ensuing discussion, the SNR level refers to any target return situated in the CUT at any point in time, whereas any other target in the reference window is considered to be an interfering target and thus denoted by the INR level. The clutter-to-noise-ratio (CNR) describes the power level at the clutter ranges, whereas interference and clutter power levels are denoted as CNR+INR. All methods compared herewith were configured to maintain $P_{fa} = 10^{-3}$ for $N = 16$. Fig. 8(b) provides the BCV trace over the entire range cells. Here, it seen that the BCV value responds effectively to the regions of homogeneity and non-homogeneity. Particularly, high BCV values were computed as expected whenever interfering targets were present in the reference window. The high BCV value about the 150th range cell clearly corresponds to the high clutter edge in the range cells. Similar to earlier observations in Section 5.1, the BCV value was effective at determining the actual number of interfering targets in the reference window in order to estimate accurate threshold values.

1. **Multiple closely spaced targets:** Fig. 9 presents an expanded view of Fig. 8(a) showing the estimated threshold values for the different methods between the 1st − 35th range cell. Three multiple closely spaced targets are located at the 25th, 27th, and 30th range cells. These targets are seen to be accurately detected by our proposed method as well as by the OS(12) and SOCA schemes. Whereas, the CA scheme failed to detect the target at the 25th range cell, while the GOCA scheme missed the targets at the 25th and 30th range cells owing to the effect of target masking. The superiority of our method can be seen in Fig. 9 following the stable threshold values estimated by our method even in the presence of the interfering targets of different INR values.
2. **Multiple targets plus clutter:** Fig. 10 shows that the target return at the 45th range cell was clearly detected by our method as well as by the SOCA scheme. The OS(12) scheme barely detected this target, whereas the CA and GOCA schemes missed the target.
   A high false alarm rate was clearly avoided by all other methods except the SOCA scheme at the first clutter edge located at the 51st range cell. The tendency of the SOCA scheme to incur an increased false alarm rate at clutter edges is well established in the theoretical literature [18]. It occurs because the lowest value from either of the leading or lagging cells is often considered to be the noise estimate by the SOCA scheme, thus leading to a lower threshold value that further increases the false alarm rate at clutter edges. However, neither of the tested methods in our experiments were able to detect the three targets embedded

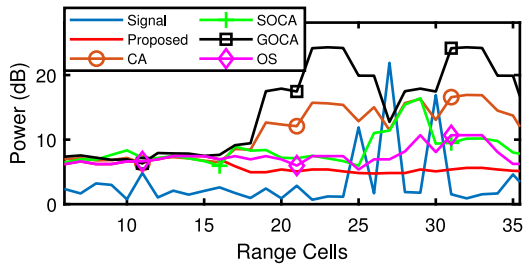

Fig. 9. Zoomed version of Fig. 8(a) showing the estimated threshold values between 1 – 35th element.

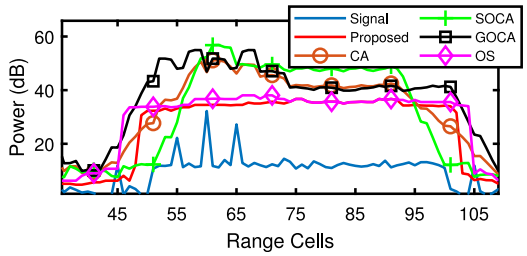

Fig. 10. Zoomed version of Fig. 8(a) showing the estimated threshold values between 41 – 110th element.

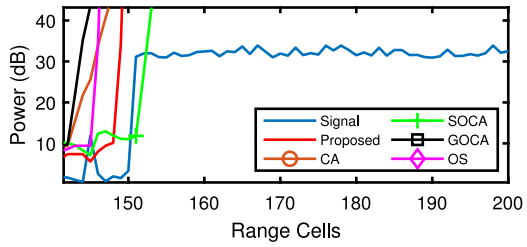

Fig. 11. Zoomed version of Fig. 8(a) showing the estimated threshold values between 130 – 172th element.

in the clutter returns at the 55th, 60th and 65th range cells. This occurred because the threshold factors used to maintain $P_{fa} = 10^{-3}$ were established based on the homogeneous noise components between the 1st – 24th range cells. Thus, since these threshold factors were maintained throughout the entire simulation and they were not readjusted automatically at the new clutter level, consequently, this led to the estimation of higher threshold values, which led to the missed targets.

3. **Target closely located to clutter edge:**
Finally, Fig. 11 shows that only our proposed method, the SOCA, and the OS(12) scheme were able to detect the target at the 145th range cell, which is closely located to the clutter edge at range cell 150. Although the CA and GOCA schemes failed to detect the target at the 145th range cell, nevertheless they maintained a low false alarm rate at the clutter edge, which is an expected result. Following these results, we have demonstrated that our method provides an improved performance as against the fixed OS scheme, the CA, GOCA, and SOCA schemes.

6. Comparison against other censoring approaches

In this section, we compare the DA-OS scheme in a quantitative sense against a notable censoring OS-CFAR scheme and then we discuss other qualities of the DA-OS scheme in comparison to other methods in the literature.

6.1. Quantitative comparison of the DA-OS scheme with the ACCA-ODV-CFAR technique

The automatic censored cell averaging (ACCA)-based ordered data variability CFAR (termed ACCA-ODV-CFAR) [26] is a popular improved version of the variability index CFAR (VI-CFAR) technique [14]. The application of a censoring mechanism using the variability index (VI) makes the ACCA-ODV-CFAR method useable when the number of interfering targets and clutter cells are unknown. In this section, we compare our DA-OS scheme against the ACCA-ODV-CFAR method. It is essential to note that the ACCA-ODV-CFAR method requires a careful fine-tuning of two highly dynamic parameters, namely, the P and the threshold parameter S. The threshold parameter S is used to decide whether the VI value stems from a homogeneous or non-homogeneous environment. Authors in [26] noted that a value of $P = 12$ should be used for a window size of $N = 16$, whereas the S parameter should be obtained via a lookup table in order to obtain its best value per iteration. Thus, in our simulation, we used $P = 12$ and then varied S in order to improve the performance of the ACCA-ODV-CFAR method. It is noted that such a fine-tuning process is not required in our DA-OS scheme, thus making it easier for use under real-life conditions.

Prior to comparing both techniques, first, we obtained the required threshold factor T used to maintain $P_{FA} = 10^{-2}$ for both techniques. This experiment was conducted under homogeneous noise-only conditions and results obtained are presented in Fig. 12(a). It can be seen from Fig. 12(a) that a similar threshold factor of $T = 1.4$ yielded $P_{FA} = 10^{-2}$ for both techniques. This value was used to compare both techniques under the case of interfering target conditions.

Fig. 12(b) presents the P_d performance under varying number of interfering targets in the lagging cells of the reference window. The target return in the CUT was maintained at SNR = 5 dB, whereas the interference-to-noise-ratio (INR) was changed from 5 dB to 10 dB. It is seen from Fig. 12(b) that the DA-OS scheme achieved a better P_d performance against the different settings of the ACCA-ODV-CFAR method. A few points are noteworthy:

1. The P_d performance of the ACCA-ODV-CFAR method increases as the S parameter is reduced. This is because more elements are classified as non-homogeneous elements as S is reduced, thus enabling the ACCA-ODV-CFAR method to detect and censor more interfering signals.
2. The P_d performance of the ACCA-ODV-CFAR method increases as INR increases. This is an expected performance since it becomes easier to detect the interfering targets as the INR is increased, which improves censoring of such interfering targets for improved P_d performance. However, there exists no further improvement in the P_d performance as S goes below 0.1 since the threshold may lie at the noise level at this point.
3. The P_d performance of the ACCA-ODV-CFAR method is grossly reduced when the number of interfering targets K in the reference window exceeds $N - P$. Thus, since $P = 12$ and $N = 16$, the actual target becomes undetectable when $K \geq 4$ as can be seen in Fig. 12(b). Such very low detection rates can be explained since the undetected interfering targets beyond $K = 4$ caused a significant bias, which led to an increase in the estimated threshold value, thus reducing the detection rate of the ACCA-ODV-CFAR method.
4. Our DA-OS scheme is invariant to an increase in the INR value. This is true since the DA-OS scheme is able to detect better the interfering targets as the INR increases, thus maintaining a high P_d performance.

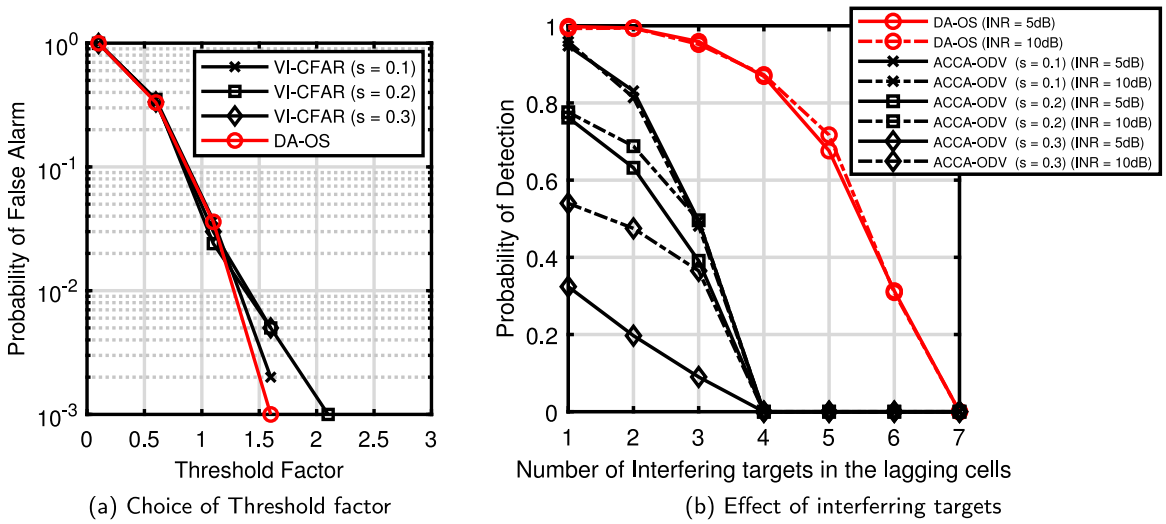

Fig. 12. (a) Choice of threshold factor to maintain a desired probability of false alarm, (b) Probability of detection under increasing number of interfering targets in the lagging cells with different INR values using N = 16 and maintaining $P_{fa} = 10^{-2}$.

5. The P_d performance of our DA-OS scheme only gradually tapers off as the number of interfering targets surpasses the lagging cells of the reference window. This demonstrates that our scheme is able to detect and censor interfering targets effectively in the reference window.

6.2. Qualitative remarks relative to other approaches

We acknowledge that there are some few notable methods in the literature deployed to estimate the *k*th element of the OS scheme and other censoring-based schemes. However, it is often difficult to compare fairly these approaches in a quantitative sense, particularly because of the absence of standardized and automated methods to accurately optimize the different parameters of these different approaches. Conducting fair comparative analysis in the absence of automated methods is further difficult owing to the dynamic nature of such parameters, for example, the threshold factor of some methods used to maintain a constant probability of false censoring must be continuously tuned per cell and per environment [13]. Thus, ensuring that such dynamic parameters are fairly optimized and fine-tuned automatically under different conditions is often a subjective and tedious trial and error process. Consequently, the need to develop standard, automated, and global parameter-tuning procedures is a concern for future works. Nevertheless, in this subsection, we make an effort to discuss some key qualitative characteristics of the DA-OS scheme relative to other known schemes (see Table 5 for a brief summary) as follows:

6.2.1. *k*th ordered element

Methods that can estimate the number of interfering targets and the *k*th element dynamically are most desired in any OS scheme. This is because such methods adapt dynamically in order to accurately censor the presence of such interfering targets as well as clutter edges in the reference window. This will improve the performance of the OS scheme. In this regard, our proposed DA-OS scheme as well as a few other notable schemes such as the AC-CFAR schemes [13,23] are able to provide such a dynamic quality.

6.2.2. Deterministic metric for homogeneity test

In order to reliably determine the presence of interfering targets and clutter edges in a reference window, it is often necessary to perform an accurate test for the degree of homogeneity/non-homogeneity of elements within the reference window. In this regard, it is much desired to obtain a metric whose value relates in a deterministic manner to the degree of homogeneity/non-homogeneity of elements in the reference window. Our DA-OS scheme presents such a well-behaved metric (i.e the BCV), which is used to accurately determine the *k*th element of the OS scheme. Prior methods such as the VI- [14], IVI- [15], and ODV-CFAR [26] schemes depend on the variability index (VI) metric in order to determine the homogeneity/non-homogeneity of elements in the reference window. However, the main limitation of the VI metric is that it depends on a threshold value whose estimate fluctuates according to the changing radar environment. This is an undesirable characteristics since there exist no practical approach to accurately determine the appropriate threshold value per environment. In our case, the BCV value is a more stable and better-behaved metric, which depends on a fixed threshold value irrespective of the operating environment.

6.2.3. Time complexity

Short computational time is most desired in any CFAR scheme. However, to the best of our knowledge, most censoring and dynamic OS schemes require a cell-by-cell processing approach in order to search accurately for the *k*th element of the OS scheme. Consequently, most methods will reduce to a TC of $O(N^2)$ since a minimum of two *for* loops will be required to process each cell as the CUT sweeps through the reference window. Our DA-OS scheme presents a similar TC, thus, it provides no significant timing advantage over other known methods.

6.2.4. Parameter tuning process

Methods with multiple parameters must be accurately fine-tuned in order to provide an improved performance. Further, such multiple parameters may require re-calibration under online operating conditions, which presents a challenge at the moment since such self-calibrating methods do not exist. Consequently, at present, methods that depend on too many parameters to be optimized are not widely desired. The DA-OS scheme does not depend on any additional dynamic parameter(s) apart from the well-known standard inputs to any CFAR scheme, which includes the reference window size and the threshold factor required to maintain a constant P_{fa} rate. This makes the DA-OS scheme a highly desirable scheme.

Table 5
Qualitative comparison of methods deployed to estimate the kth rank ordered element of the OS scheme.

Method	Year	kth ordered element	Deterministic metric for homogeneity test	Time complexity	Requires parameter tuning process	Uses P_{fc} lookup table	Number of schemes
AC-CFAR [23]	1992	Dynamic	No	$O(N^2)$	Yes	Yes	Single
GOSGOSO [19]	1995	Fixed	No	$O(N^2)$	Yes	Yes	Multiple
VI-CFAR [14]	2000	NA	Yes	$O(N^2)$	Yes	Yes	Multiple
IVI-CFAR [15]	2004	Fixed	Yes	$O(N^2)$	Yes	Yes	Multiple
ACCA-ODV [26]	2005	Fixed	Yes	$O(N^2)$	Yes	Yes	Single
ADCCA-CFAR [12]	2008	Fixed	Yes	$O(N^2)$	Yes	Yes	Single
AC-CFAR [13]	2014	Dynamic	No	$O(N^2)$	Yes	Yes	Multiple
Proposed DA-OS	2020	Dynamic	Yes	$O(N^2)$	No	No	Single

6.2.5. Use of P_{fc} lookup table

In the absence of tractable mathematical methods to maintain a constant probability of false censoring (P_{fc}), most known methods must depend on a lookup table in order to select an appropriate censoring threshold value per changing environment (see Table 5). In addition to being a cumbersome and often inaccurate approach, the use of lookup tables introduces additional memory requirements for radar systems, which is an undesirable characteristic. Our DA-OS scheme presents an advantage since it does not depend on any lookup table for its censoring process.

6.2.6. Number of schemes

Some censoring methods are designed to switch between multiple CFAR schemes based on the outcome of some test result(s) [13–15]. However, such a switching architecture introduces additional design complexities including the need to construct multiple schemes within a radar sensor. Such a characteristic is often undesirable since certain applications may be limited in both computing resources and physical space. Consequently, single CFAR schemes such as our DA-OS scheme are most desired in radar systems.

Essentially, we have argued based on the foregoing that our DA-OS scheme presents a number of desirable characteristics as against other schemes. Thus, the DA-OS scheme will be beneficial to many applications that depend on effective CFAR schemes for improved performance. In particular, it could possibly be applied to vector adaptive detection applications, where square law operations are not performed in the detection chain, instead, the multidimensional space can be explored to improve radar detection [36,37].

7. Conclusion

We have proposed a method that determines automatically and effectively the kth rank ordered element of the ordered statistics (OS) CFAR scheme based on the principle of discriminant analysis. Our method computes the between-class variance (BCV) value of each cell in the reference window towards determining the degree of homogeneity and non-homogeneity of radar returns within the reference window. It then uses the BCV value to estimate the number of interfering targets in the reference window, thus determining the kth rank ordered element of the scheme. We have shown that our approach is effective under a number of different environments, including under homogeneous and non-homogeneous conditions. Thus, following the results obtained, our method maintains a high detection rate amidst multiple interfering targets, it exhibits a very low CFAR loss in homogeneous conditions, and reduces the false alarm rate at clutter edges compared to existing methods. A main limitation of the proposed method is its increased computational complexity as against some classic methods such as the CA, GOCA, SOCA, and fixed OS schemes. Nevertheless, the DA-OS scheme will be of great benefit to a number of remote sensing applications, particularly where increased radar performance is required alongside other desired characteristics as summarized in Table 5. A few areas recommended for future works include reducing the computational complexity of the proposed algorithm for faster realtime operation, detecting the case of multiple clutters in a reference window, and extending the present one dimensional data structure of the BCV value to the case of a two dimensional structure, which will greatly benefit image processing applications, such as in satellite and geographical-based remote sensing applications.

CRediT authorship contribution statement

A.J. Onumanyi: Conceptualization, Methodology, Software, Writing - original draft. **H. Bello-Salau:** Formal analysis, Writing - review & editing. **A.O. Adejo:** Investigation, Writing - review & editing. **H.O. Ohize:** Visualization, Writing - review & editing. **M.O. Oloyede:** Validation, Writing - review & editing. **E.N. Paulson:** Validation, Writing - review & editing. **A.M. Aibinu:** Supervision, Writing - review & editing.

Declaration of competing interest

The authors declare that they have no known competing financial interests or personal relationships that could have appeared to influence the work reported in this paper.

References

[1] G. Mosqueira, J. Apetz, K. Santos, E. Villani, R. Suterio, L. Trabasso, Analysis of the indoor GPS system as feedback for the robotic alignment of fuselages using laser radar measurements as comparison, Robot. Comput.-Integr. Manuf. 28 (6) (2012) 700–709.
[2] F. Wang, Y. Wang, J. Liu, Y. Wang, The feature recognition of CFRP subsurface defects using low energy chirp-pulsed radar thermography, IEEE Trans. Ind. Inf. (2019) 1.
[3] M. Geiger, C. Waldschmidt, 160-GHz radar proximity sensor with distributed and flexible antennas for collaborative robots, IEEE Access 7 (2019) 14977–14984.
[4] S.D. Blunt, P. Yatham, J. Stiles, Intrapulse Radar-Embedded Communications, Vol. 46, 2010, pp. 1185–1200.
[5] D. Ciuonzo, A.D. Maio, G. Foglia, M. Piezzo, Intrapulse radar-embedded communications via multiobjective optimization, IEEE Trans. Aerosp. Electron. Syst. 51 (4) (2015) 2960–2974.
[6] M. Min, J. Li, F. Wang, Z. Liu, W. Menzel, Retrieval of cloud top properties from advanced geostationary satellite imager measurements based on machine learning algorithms, Remote Sens. Environ. 239 (2020) 111616.
[7] M. Weiss, F. Jacob, G. Duveiller, Remote sensing for agricultural applications: A meta-review, Remote Sens. Environ. 236 (2020) 111402.
[8] P. Chernyshov, T. Vrecica, M. Streßer, R. Carrasco, Y. Toledo, Rapid wavelet-based bathymetry inversion method for nearshore X-band radars, Remote Sens. Environ. 240 (2020) 111688.
[9] A. Freeman, M. Zink, E. Caro, A. Moreira, L. Veilleux, M. Werner, The legacy of the SIR-C/X-SAR radar system: 25 years on, Remote Sens. Environ. 231 (2019) 111255.

[10] M. Arik, O.B. Akan, Realizing joint radar-communications in coherent MIMO radars, Phys. Commun. 32 (2019) 145–159.
[11] M. Arik, O.B. Akan, Capacity analysis for joint radar-communication capable coherent MIMO radars, Phys. Commun. (2020) 101062.
[12] A. Zaimbashi, Y. Norouzi, Automatic dual censoring cell-averaging CFAR detector in non-homogenous environments, Signal Process. 88 (11) (2008) 2611–2621.
[13] N. Boudemagh, Z. Hammoudi, Automatic censoring CFAR detector for heterogeneous environments, AEU-Int. J. Electron. Commun. 68 (12) (2014) 1253–1260.
[14] M.E. Smith, P.K. Varshney, Intelligent CFAR processor based on data variability, IEEE Trans. Aerosp. Electron. Syst. 36 (3) (2000) 837–847.
[15] Z. Hammoudi, F. Soltani, Distributed IVI-CFAR detection in non-homogeneous environments, Signal Process. 84 (7) (2004) 1231–1237.
[16] M. Weiss, Analysis of some modified cell-averaging CFAR processors in multiple-target situations, IEEE Trans. Aerosp. Electron. Syst. (1) (1982) 102–114.
[17] R. Srinivasan, Robust radar detection using ensemble CFAR processing, IEE Proc. Radar Sonar Navig. 147 (6) (2000) 291–297.
[18] P.P. Gandhi, S.A. Kassam, Analysis of CFAR processors in homogeneous background, IEEE Trans. Aerosp. Electron. Syst. 24 (4) (1988) 427–445.
[19] H. You, H. Rohling, Performance of two generalized order statistics CFAR detectors with automatic censoring technique in multiple target situations, J. Electron. (China) 12 (1) (1995) 38–47.
[20] G.M. Hatem, T.R. Saeed, J.W. Sadah, Comparative study of combined CFAR algorithms for non-homogenous environment, Procedia Comput. Sci. 131 (2018) 58–64.
[21] G.V. Weinberg, Interference control in sliding window detection processes using a Bayesian approach, Digit. Signal Process. (2020) 102658.
[22] H. Rohling, New CFAR-processor based on an ordered statistic, in: International Radar Conference, 1985, pp. 271–275.
[23] S.D. Himonas, M. Barkat, Automatic censored CFAR detection for nonhomogeneous environments, IEEE Trans. Aerosp. Electron. Syst. 28 (1) (1992) 286–304.
[24] L. Prastitis, J. Frank, S. Himonas, Automatic censored cell averaging CFAR detector in nonhomogeneous clutter, in: 92 International Conference on Radar, IET, 1992, pp. 218–221.
[25] R. Ghosh, A. Vajpeyi, A. Akula, V. Shaw, S. Kumar, H. Sardana, Performance evaluation of a real-time seismic detection system based on CFAR detectors, IEEE Sens. J. (2019).
[26] A. Farrouki, M. Barkat, Automatic censoring CFAR detector based on ordered data variability for nonhomogeneous environments, IEE Proc. Radar Sonar Navig. 152 (1) (2005) 43–51.
[27] Y. He, Performance of some generalised modified order statistics CFAR detectors with automatic censoring technique in multiple target situations, IEE Proc. Radar Sonar Navig. 141 (4) (1994) 205–212.
[28] M.A. Richards, Fundamentals of Radar Signal Processing, Tata McGraw-Hill Education, 2005.
[29] F. Gini, F. Lombardini, L. Verrazzani, Decentralized CFAR detection with binary integration in Weibull clutter, IEEE Trans. Aerosp. Electron. Syst. 33 (1997) 396–407.
[30] D. Ciuonzo, A.D. Maio, P.S. Rossi, A systematic framework for composite hypothesis testing of independent Bernoulli trials, IEEE Signal Process. Lett. 22 (9) (2015) 1249–1253.
[31] N. Otsu, A threshold selection method from gray-level histograms, IEEE Trans. Syst. Man Cybern. 9 (1) (1979) 62–66.
[32] A.J. Onumanyi, E.N. Onwuka, A.M. Aibinu, O.C. Ugweje, M.J.E. Salami, A modified Otsu's algorithm for improving the performance of the energy detector in cognitive radio, AEU-Int. J. Electron. Commun. 79 (2017) 53–63.
[33] S. Saliu, A.J. Onumanyi, J.A. Abolarinwa, Performance analysis of a modified otsu-based constant false alarm rate (CFAR) algorithm under varying signal to noise ratio in radar systems, in: Proceedings of ICGET 2018, 2018, pp. 110–114.
[34] V.H. Thanh, R. Zunino, C. Priami, Efficient constant-time complexity algorithm for stochastic simulation of large reaction networks, IEEE/ACM Trans. Comput. Biol. Bioinf. 14 (3) (2017) 657–667.
[35] B. Chandramouli, J. Goldstein, Patience is a virtue: Revisiting merge and sort on modern processors, in: Proceedings of the 2014 ACM SIGMOD International Conference on Management of Data, ACM, 2014, pp. 731–742.
[36] C. Hao, D. Orlando, G. Foglia, G. Giunta, Knowledge-based adaptive detection: Joint exploitation of clutter and system symmetry properties, IEEE Signal Process. Lett. 23 (10) (2016) 1489–1493.
[37] D. Ciuonzo, A.D. Maio, D. Orlando, A unifying framework for adaptive radar detection in homogeneous plus structured interference— part II: Detectors design, IEEE Trans. Signal Process. 64 (11) (2016) 2907–2919.

Dr. Adeiza James Onumanyi received his Bachelor of Engineering degree in Electrical and Electronics Engineering from the Abubakar Tafawa Balewa University, Bauchi, Nigeria in 2005, and his Master of Engineering, and Doctor of Philosophy degrees in Communication Engineering from the Federal University of Technology (F.U.T), Minna, Nigeria in 2010 and 2014, respectively. Dr. Onumanyi was a postdoctoral research fellow at the University of Pretoria, South Africa. He has published several research articles in different peer reviewed journals, and in different IEEE flagship conferences. He lectures at the Department of Telecommunication Engineering, F.U.T, Minna, Nigeria. He has won several grants at F.U.T, Minna, served on several organizing committees for different conferences including IEEE conferences, reviewed several articles for high impact journals and he has participated in different technical workshops. His research interests include spectrum sensing in cognitive radio, wireless sensor networks, radar systems, image processing, cyber physical systems and low powered wireless area networks.

Dr. H. Bello-Salau obtained a B.Tech degree in Electronic/Electrical Engineering from Ladoke Akintola University of Technology Ogbomoso, Nigeria in 2009. He proceeded to International Islamic University Malaysia, Kuala-Lumpur where he received M.Sc degree in Communication Engineering in 2012. He obtained his Ph.D degree in Communication Engineering from the Federal University of Technology Minna, Nigeria in 2017. He currently works at the Department of Computer Engineering, Ahmadu Bello University, Zaria, Nigeria. He has authored and co-authored more than 20 different research articles in peer reviewed journals and over 30 conference articles. His research interest includes Digital Signal and Image Processing, Vehicle Ad-Hoc Networks, Artificial Intelligence, Cognitive Radio and Wireless Sensor Networks.

Dr. Achonu Adejo has a first degree in Electrical/Computer Engineering from Federal University of Technology Minna, Nigeria obtained in 2006, an M.Sc. from University of Nottingham (Malaysia campus) in 2010 and a Ph.D. in Electrical Engineering from Newcastle University, UK in 2018. His doctorate program was carried out in the Communications, Sensors and Signal processing group at the School of Engineering. Since 2010, he has been with Federal University of Technology Minna. His current research interests are in Resource management and modelling of Cellular communications with focus on 5G communications and D2D networks.

Dr. Henry Ohize earned a Ph.D. in 2017 from the University of Cape Town, South Africa, a master's degree in Telecommunication Engineering from Federal University of Technology Minna, Nigeria in 2010 and a Bachelor's degree in Electrical and Electronics Engineering, from the Abubarkar Tafawa Balewa University Bauchi, Nigeria in 2005. He is currently a senior lecturer at the Federal University of Technology, Minna. His research interests include, the full realization and implementation of 5G technology: Cognitive Radio, Wireless Sensor Networks, MIMO, mmWave and 5G application areas.

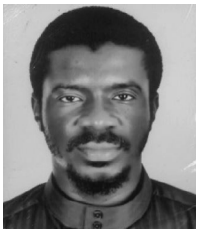

Dr. Muhtahir O. Oloyede received the B.Eng. degree in Electrical Engineering from the University of Ilorin, Nigeria, and the M.Sc. degree in Information Systems from the University of East London, U. K. in 2011. He earned a Ph.D. degree in Electrical, Electronic and Computer Engineering from the University of Pretoria in 2019. His research interests include application of biometric sensing systems, image processing, computer vision, data fusion, and detection recognition algorithms.

Eberechukwu N. Paulson received his Bachelors in Engineering degree (Electrical and Electronics) in 2012 from the Federal University of Technology, Akure, Ondo state, (Nigeria's topmost University of Technology). He obtained his Master of Engineering degree (Telecommunications and Electronics) in 2017 with a distinction and a recipient of the Best Post-Graduate Student Award from the prestigious Universiti Teknologi Malaysis (UTM), Johor, Malaysia. He is currently pursuing the Doctor of Philosophy degree with the School of Electrical Engineering, UTM. His general research interest lies in the field of wireless communications, computer networking system design, and optimization. In particular, he is interested in Software Defined Networks (SDN), Internet of Things (IoT), Cognitive Radio Networks (CRN), and Wireless Sensor Networks (WSN).

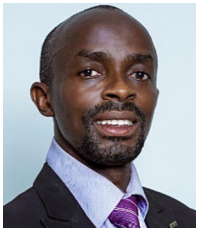

Professor Abiodun Musa Aibinu is a highly-motivated career driven achiever with over Eighteen (18) years working experience in the field of: Information and Communication Technology (ICT); Robotics, Mechatronics Engineering, Telecommunication Engineering, Project Management, Spectrum Management, Industrial Automation, Teaching and Research in the field of Artificial Intelligence, ICT and Robotics. He received: National Diploma award from The Polytechnic, Ibadan, Nigeria;B.Sc. degree from Obafemi Awolowo University (OAU), Ile-Ife, Nigeria; M.sc degree from Blekinge Institute of Technology (BTH), Sweden and Doctoral degree from International Islamic University Malaysia, (IIUM), Malaysia. He has authored and co-authored several publications in both local and international journals and conferences. Some of his published work are highly cited in the academic field. He is presently the Head of Department, Mechatronics Engineering Department, FUT Minna, and the Director, Center for Open Distance and e-Learning (CODeL), FUT Minna. He is also the pioneer and coordinator of Advanced Engineering Innovation Research Group. Professor Aibinu is a registered Engineer with COREN and NSE. His research interests include: Digital signal and Image processing; Instrumentation and measurement; Intelligent system design and artificial intelligence with emphasis on artificial neural networks and Genetic Algorithm.